Link Analysis for the LRPT Digital Weather Satellite System

Roger A. Dalke
Robert J. Achatz
Christopher L. Holloway
George A. Hufford
Edmund A. Quincy

CONTENTS

CONTENTS (Cont'd)

Page

LINK ANALYSIS FOR THE LRPT DIGITAL WEATHER SATELLITE SYSTEM

R. Dalke, R. Achatz, C. Holloway, G. Hufford, and E. Quincy[*]

The National Oceanic and Atmospheric Administration, the European Space Agency, and the European Organization for the Exploitation of Meteorological Satellites are designing a weather satellite system that will broadcast digital weather images at VHF. As a part of that effort, the Institute for Telecommunication Sciences has analyzed the VHF digital communications link. The results of the link analysis are described in this report. This analysis is based on published literature and models that describe propagation effects such as ionospheric scintillation and man-made noise, and are applicable to VHF digital communications. The analysis includes the estimation of the required link margins for coded binary and quaternary phase-shift modulation methods.

Key words: VHF satellite communications; VHF digital communications; man-made noise; ionospheric scintillation; meteorological satellites; weather satellite images; low rate picture transmission (LRPT); automatic picture transmission (APT); television infrared observation satellite (TIROS)

1. INTRODUCTION

In 1963, the United States launched polar orbiting weather satellites that transmit images of the earth using an FM broadcast at radio frequencies between 137 and 138 MHz. This broadcast system is called the automatic picture transmission (APT) system and was used originally by U.S. weather offices. Plans for building relatively simple, low-cost ground receiving stations were widely distributed to meteorological services worldwide. Since that time, activity and interest in receiving the direct readout images has increased significantly. Currently, there are plans to upgrade the APT system to digital technology, which is referred to as the low rate picture transmission (LRPT). Design decisions will require a detailed analysis of VHF propagation effects, noise environment, receiving site environment, and their effects on received picture quality.

This report details a study of the VHF satellite-to-ground propagation channel and its effects on the proposed LRPT digital broadcast system. Technical specifications used in this study (e.g., transmitter, bandwidth, modulation, and receivers) are based on both the existing APT system and the proposed LRPT system. The link analysis was divided into scenarios based on the type of earth station receiving system (low-end, high-end) and the satellite receiver path geometry that would give the maximum received signal strength (satellite at zenith) and the minimum signal strength with the satellite in view (minimum specified elevation). In addition, four different man-made noise environments were addressed. The specifications for these different cases and the analysis of the satellite-to-earth link are detailed in the report.

---

[*] The authors are with the Institute for Telecommunication Sciences, National Telecommunications and Information Administration, U.S. Department of Commerce, Boulder, CO 80303

The analysis of the space-to-earth link requires consideration of the link path geometry and the effects of the ionosphere and troposphere on the radio signal. At the frequency of interest (137 MHZ), the signal will easily penetrate the ionosphere, however, one must consider the deleterious effects of ionospheric scintillation. In general, scintillation is not an important factor at midlatitudes. Scintillation can be significant, however, when the radio link path traverses sections of the ionosphere above the magnetic equatorial and polar regions of the earth where fades exceeding 10 dB can be experienced. At the frequency of interest, the troposphere has little effect on the signal. The effects of both the ionosphere and the troposphere are discussed in this report.

Knowledge of the level of external radio noise at the receiver is essential for system design. Radio noise originates from both natural and man-made sources. Natural radio noise considered in this analysis is primarily due to heavenly bodies (e.g., sun, planets, and stars). In populated areas at 137 MHZ, noise originating from human activities typically dominates the natural radio noise background. In this Study, we considered both sources of noise and their effects on the link requirements.

In Section 2 we define the radio link geometry and relevant link equations. We also identify and characterize two representative combinations of earth station (E/S) equipment that are used in the link calculations. Section 3 focuses on the propagation effects introduced by the ionosphere and troposphere that affect link budget calculations and overall system performance. The noise environment for this system is analyzed in Section 4, where we calculate predicted noise levels based on published noise measurements in four different man-made noise environments. Based on these results, the received carrier-to-noise ratio (CNR) for each noise environment and E/S receiver system is tabulated. We also have reviewed proposed digital modulation schemes and their performance in terms of CNR required to achieve specified bit-error-ratios (see Section 5). The results of the link budget calculations are tabulated in Appendix A. Here we provide tables detailing the link calculation and the resulting link margin based on the required CNR for two modulation schemes. The cumulative distribution (time availability) of the CNR for 5-W and 15-W transmitters, the low-end and high-end receiving system, and the four noise environments are also given in Appendix A

2. SPACE-TO-EARTH LINK ANALYSIS

In this section we introduce the link equations needed to calculate the CNR ratio. We also specify the receiver and antenna characteristics for the low-end and high-end receiving systems evaluated in this report.

2.1 Equations for Received Power and Noise Power

The received power at the output terminals of the receiving antenna is given by [1]:

$$P_r = EIRP + G_r - L_{fs} - A \ (dBW) \tag{1}$$

where EIRP is the effective isotropic radiated power, the product of the transmitter antenna gain, and the effective (including system losses) transmitter power; G_r, is the receiver gain; and L_{fs} is the free space or basic transmission loss:

$$L_{fs} = 32.45 + 20\log F_{MHz}R_{km} \ (dB) , \tag{2}$$

where R_{km} is the path distance (in km) and F_{MHz} is the frequency (in MHz). *A* represents path attenuation resulting from propagation in a lossy medium. The effects of propagation in the troposphere and ionosphere (including ionospheric scintillation) are discussed in Section 3 of this report.

The CNR is given simply as the ratio of the received signal at the terminals of the receiving antenna to the system noise power referenced to the same point in the receiving system:

$$CNR = P_r - 10\log(kb) - 10\log (T_{sys}) \ (dB) , \tag{3}$$

where k is Boltzmann's constant (1.380662×10^{-23} J/K), b is the noise equivalent bandwidth of the receiver (72 kHz for the proposed LRPT), and T_{sys} is the system noise temperature and is defined in Equation (6) below.

In the link calculations that follow, we have assumed two values for the transmitter output power: 5 W and 15 W. Losses for the transmitting satellite system are assumed to be 2.2 dB [2] (this includes antenna circuit losses, polarization mismatch, transmission line losses, etc.)

2.2 Earth Station Receiving Systems

For the purposes of this study, two archetypal E/S receivers are defined; a low-end system and a high-end system. The high-end system consists of a high-gain tracking antenna combined with a high quality receiver having a noise figure of 1 dB. The low-end system consists of an "omnidirectional" antenna combined with an average quality receiver having a noise figure of 6 dB.

The typical high-end antenna is a crossed Yagi-Uda with a gain of about 10 dB as described by Summers [3]. For the purposes of the link calculations, we have approximated the directive gain for this antenna by using a published antenna pattern for a Yagi-Uda antenna with roughly the same features (e.g., number and size of elements) [4]. The pattern is shown in Figure 1. To approximate a crossed Yagi-Uda, we assumed that the pattern was rotationally symmetric. The resulting gain is somewhat higher than 10 dB, but should provide a reasonable approximation for the purposes of noise calculations. Since the high-end system tracks the satellite, the receiver gain (G_r) does not depend on the satellite elevation (here $G_r = 10$ dB).

The typical "omnidirectional" antenna is a half wavelength VHF Volute. The pattern is shown in Figure 2 [2]. The Volute antenna is not steerable; hence, the low-end system receiver gain varies with elevation angle as shown in Figure 2. For each system (high/low-end receivers), link calculations were made for the greatest and the least free space path loss with the satellite within the specified viewing elevation angles. The greatest path loss occurs at the lowest elevation angle for which the system is required to achieve the specified link margin: 5° for the high-end system and 13° for the low-end system. The least path loss occurs at zenith.

2.3 Satellite Location

Effective radiated isotropic power is a function of the transmitting antenna gain G_t and the satellite look angle α. The satellite look angle α is defined in Figure 3 and is determined by the following expression:

$$\alpha = \sin^{-1}\left(\frac{r_e \cos(EL)}{r_s}\right),$$ (4)

where

$$r_s = r_e + Altitude,$$ (5)

where r_e is the radius of the earth (6370 km) and A is the altitude of the satellite (824 km). For the three elevation angles of interest (90°, 13°, and 5°), the corresponding look angles are 0°, 60°, and 62°, respectively. The gain of the satellite antenna as a function of look angle is determined from the transmitting antenna pattern shown in Figure 3 [5]. The gains for the three look angles of interest are 3.7, 0, and -0.3 dB, respectively (Figure 4).

The distance to the satellite as a function of elevation angle is given by:

$$R = [r_s^2 + r_e^2 - 2r_e r_s \cos(\frac{\pi}{2} - EL - \alpha)]^{\frac{1}{2}}$$ (6)

which, for the elevation angles of interest is 824, 2207, and 2833 km respectively.

2.4 Directional and Path Length Variations Due to the Troposphere

The ray path through the troposphere is curved due to refraction. Because of the curvature of the path, the direction to the satellite is different from the geometric direction. This change in the path direction changes both the satellite look angle and distance to the satellite. Based on expressions
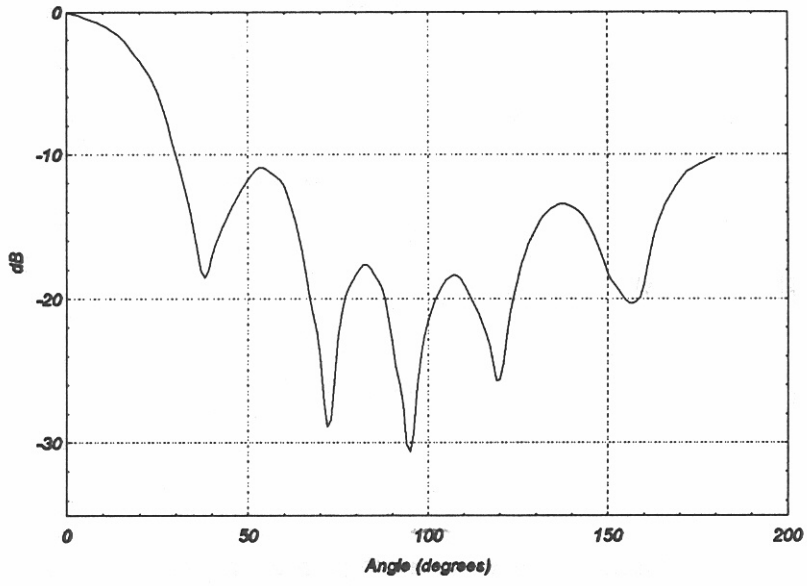
4

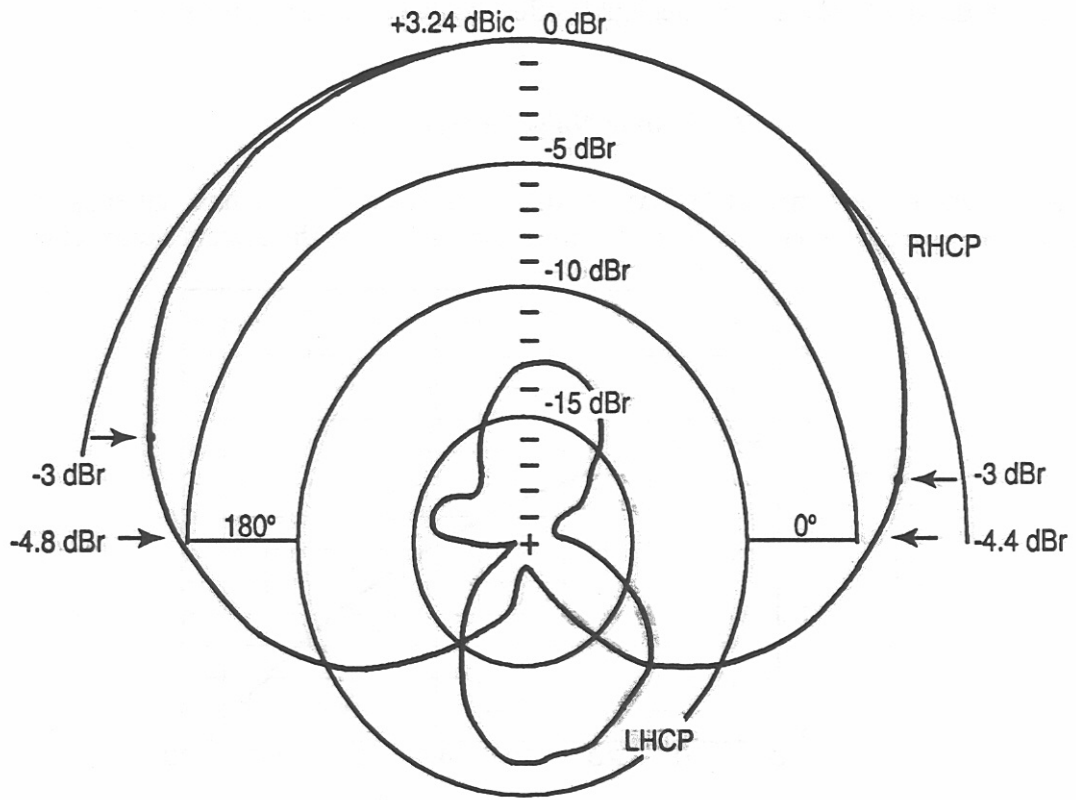Figure 1. Pattern for a six-element Yagi-Uda antenna.

Figure 2. Volute antenna pattern.
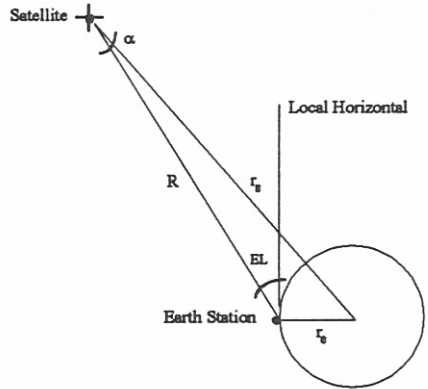
Figure 3. Space-to-earth path geometry.

given in [6] and an operating frequency of 137 MHz, the largest change in elevation angle is less than one tenth of a degree and the largest change in path length is 28 m (both occur at an elevation angle of 5°), hence, the troposphere has a negligible effect on the received signal power.

2.5 System Noise Temperature

The total system noise temperature has contributions from the antenna, antenna circuit and transmission line, and the receiver. The following expression for the system noise temperature is

Figure 4. Satellite transmitter antenna pattern.

6

referenced to the receiving antenna terminals:

$$T_{sys} = T_a + (L-1)T_0 + LT_r$$

(7)

$$T_r = T_0(10^{\frac{NF}{10}} - 1)$$
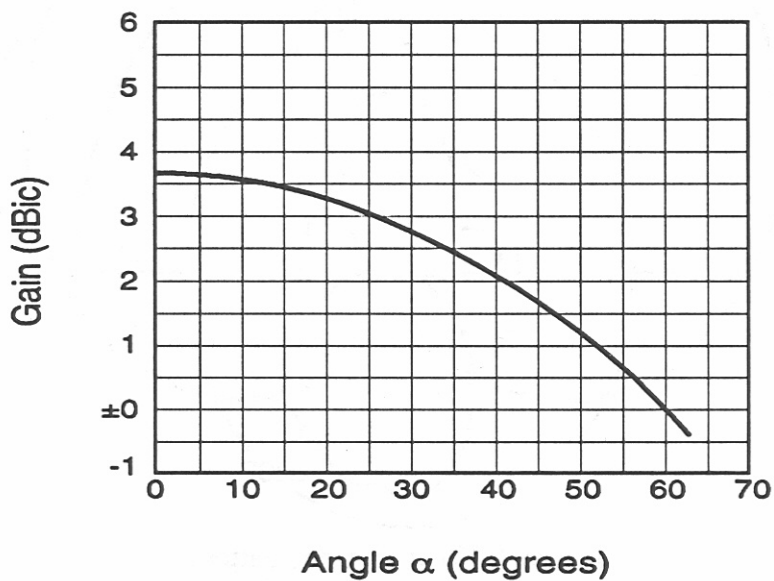
where L represents E/S losses (e.g., antenna circuit, polarization mismatch, and transmission line losses), T_0 is the ambient temperature (290 K), NF is the noise figure of the receiver, and T_a is the antenna temperature. The antenna temperature is due to both natural and man-made noise sources which are analyzed in detail in Section 4. The temperature of the low-end earth station receiver is 865 K and the high-end earth station is 75 K. For the purposes of this analysis, the earth station losses were assumed to be 2 dB (receiver implementation losses not including demodulation losses) [7].

3. PROPAGATION EFFECTS

The transmitted power arrives at the receiver at greatly reduced levels, primarily because of the spherical spreading of the radio wave. This "free space loss" for the space-to-earth propagation path will equal about 135 dB. In addition, however, the radio wave must travel through the atmosphere and then possibly through obstacles on the ground. In some circumstances, this can lead to further losses of tens of decibels. Many of these circumstances are easily avoidable and should not be designed against. It seems folly, for example, to attempt reception where there is no clear view of the sky, at street level in a downtown urban area, or at the bottom of a deep canyon. Other circumstances, however, require some planning if they are to be avoided. Tropospheric and ionospheric effects are discussed below.

3.1 Tropospheric Effects

The lowest 10 km or so of the atmosphere is the troposphere. Its major constituents are the gases nitrogen, oxygen, and water vapor. These combine to give it an *index of refraction n.* At standard conditions, this index has a value of about 1.000300, and it always differs only slightly from unity. For this reason, one usually resorts to discussions of the *refractivity $N = n–1$* and measures that quantity in parts per million or, as the engineers prefer to say, *N-units.* In a standard atmosphere, then, the refractivity has a sea level value of about 300 N-units and decreases exponentially with altitude, having a scale height of about 7.5 km. Although the numbers involved here are small, they sometimes have important consequences. For example, since the refractivity decreases with height, radio waves tend to bend down towards the ground. On terrestrial paths, this extends the horizon, a fact that can be accounted for by pretending (under the standard conditions given above) that the earth's radius is 4/3 its actual value. On satellite paths, however, the waves will leave the atmosphere before they have suffered much bending. A ray leaving the earth at an elevation angle of 5° will, when it exits the troposphere, have changed its direction by about 2 mrad (0.1°).

7

In general, the refractivity is a function of pressure, temperature, and humidity, and therefore a function of the weather (see e.g., [8, 9, 10]). When the atmosphere is well mixed (as is the normal condition and especially so during storms) the refractivity is a well-behaved function of position and will resemble the "standard" atmosphere described above. But a stable atmosphere often means trouble because, the refractivity is horizontally stratified and can vary with height in quite abnormal ways. The most severe possibility occurs when an *atmospheric duct* forms, in which radio waves bend downwards and are "trapped" close to the earth's surface so that they may travel a considerable distance. The occurrence of these ducts often is related to the "inversion layers" so frequently lamented.

Actually, however, a ray will "penetrate" such ducts even at fairly small angles of elevation. The rule of thumb is that rays steeper than 30 will be unaffected by any stratified atmosphere. Thus, satellite reception, even at 5° above the horizon, should be unaffected.

On the other hand, there may be instances of *unintended* reception. A satellite may be below the horizon while its signal is carried by a duct directly to the receiver. If this is an unwanted signal from a separate service, it may become deleterious interference. In the case of reception of the desired satellite, the signal may be received unexpectedly (i.e., early), fadeout, and after a wait, reappear and behave as expected.

Molecular absorption (by oxygen or water vapor) and rain attenuation is, at these frequencies, too small to measure. Even obstacle losses (when, say, a building or a tree canopy intersects the radio path) and penetration losses (when the receiver is inside a building) might be only a few decibels, depending on the exact geometry. While avoiding such losses will certainly improve the system's efficiency, there may be situations where they cannot be avoided and where the losses will still be tolerable.

Another situation that one should try to avoid is that in which "multipath" might degrade reception. Reflections from buildings or scattering from trees can introduce additional radio paths that might interfere destructively with the direct path. A building *behind* the receiver is particularly troublesome. Proposed bandwidths are small enough that fading will not be frequency selective, but the remaining flat fading can easily exceed 10 dB. Because the satellite moves, the fading will be dynamic. If such behavior is unavoidable, perhaps space diversity will be useful.

3.2 Ionospheric Effects

The ionosphere is that part of the atmosphere that exists from perhaps 70-1000 km above the earth. The air here is very tenuous and the sun's rays strip electrons from the molecules forming a plasma of positively charged ions and negatively charged free electrons. It is these free electrons that interact with radio waves and can cause deviations from free-space transmission. One speaks of an "effective refractivity" having the form (at high frequencies) $N = -40.3\ N_e/f^2$, where N_e is the electron density

and f the radio frequency in Hz. At 137 MHz and the densest part of the ionosphere (the F-layer with. $N_e=1.6\times10^{12}/m^3$), N has the value -0.003. Not only is this negative (so that the phase velocity is greater than it is in free space) but its magnitude is much larger than the refractivity of the troposphere.

Thus, the frequency of 137 MHz is high enough that the waves will easily penetrate the ionosphere, but not high enough that this penetration will be unaffected. But there are times when the free electrons form into generally irregular clouds and blobs. This makes the effective index of refraction similarly irregular so that a kind of diffractive screen forms and the received signal level may deviate from the assumed free-space level. The irregularities change with time so that the received signal changes with time and one says that it "scintillates." The central value is still the computed free-space value, and deviations (at 137 MHz) might be 10 dB or more. Of course, 10 dB *more* signal will not be a problem, but the loss of 10 dB will usually be disastrous. The temporal variation is that of a stochastic process with frequency components beginning to disappear at about 1 Hz. Fadeouts exceeding 3 dB have an average duration of maybe 1 s.

These effects are largely dependent on the earth's magnetic field. They appear mostly within about 30° of the magnetic poles or 20° of the geomagnetic equator. Midlatitudes usually are free of any significant effects. Figure 5 delineates the areas of possible concern (except for the rare occurrence of a fierce magnetic storm). In addition, there are strong yearly, seasonal, and diurnal variations. In the equatorial region, scintillation appears almost entirely at night between, say, between 1000 and 0500 hours. It is twice as strong during equinoctial periods as during the solstices. It is highly dependent on solar activity, showing much greater effects during sunspot maxima as during sunspot minima. In the auroral regions, there are two important parts of the ionosphere: the "polar cap" and the "auroral oval." The polar cap appears directly over the magnetic pole and is almost always there.
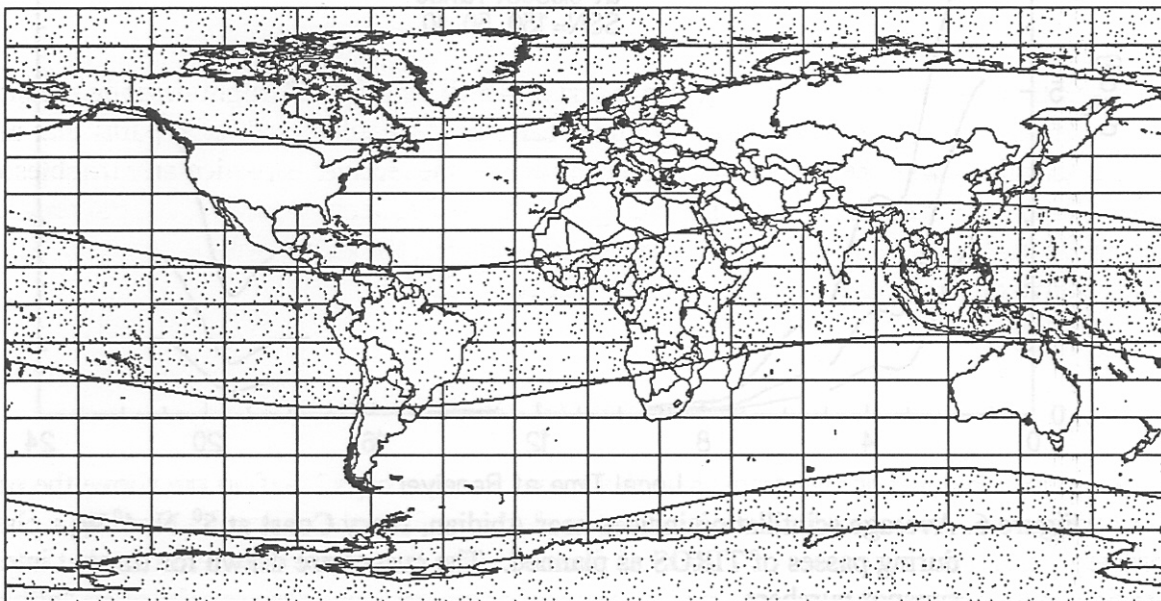

Figure 5. Regions of the world where ionospheric scintillation might be significant (shaded areas).

Only during the summer (when the sun shines all night long) does scintillation tend to disappear. At all other times, it seems to be independent of the hour and of solar activity. The auroral oval is a ring about 20° or 25° away from the pole. This is the ring that receives a rain of particles from the sun and responds with the awesome auroral displays. The resulting radio scintillation is strongest at night and depends strongly on sunspot number.

To illustrate what might happen, Figures 6 through 10 show the average standard deviations σ_x of received signal levels from simulated weather satellite (TIROS) passes. Receiver sites were selected for their relation to the phenomena, while the satellite was placed at the point (in any one pass) is nearest to the receiver. The orbits are sun synchronous so that their ascending nodes (for example) occur always at the same local time. However, the longitudes of these nodes may appear anywhere along the equator, and for our purposes were assumed to be random and uniformly distributed. The short segments in the figures show the consequent scintillation indices at the times the two satellites passed over the receiver. Three sunspot numbers were used: 150, a near maximum; 50, an average number; and 10, a near minimum. At Washington (Figure 7), however, the scintillation was not only very small; it was independent of sunspot number. The three northern cities (Figures 8-10) exhibited varying degrees of alarming results. While the standard deviations are rarely larger than 4 dB, they can have sensible values at any time.

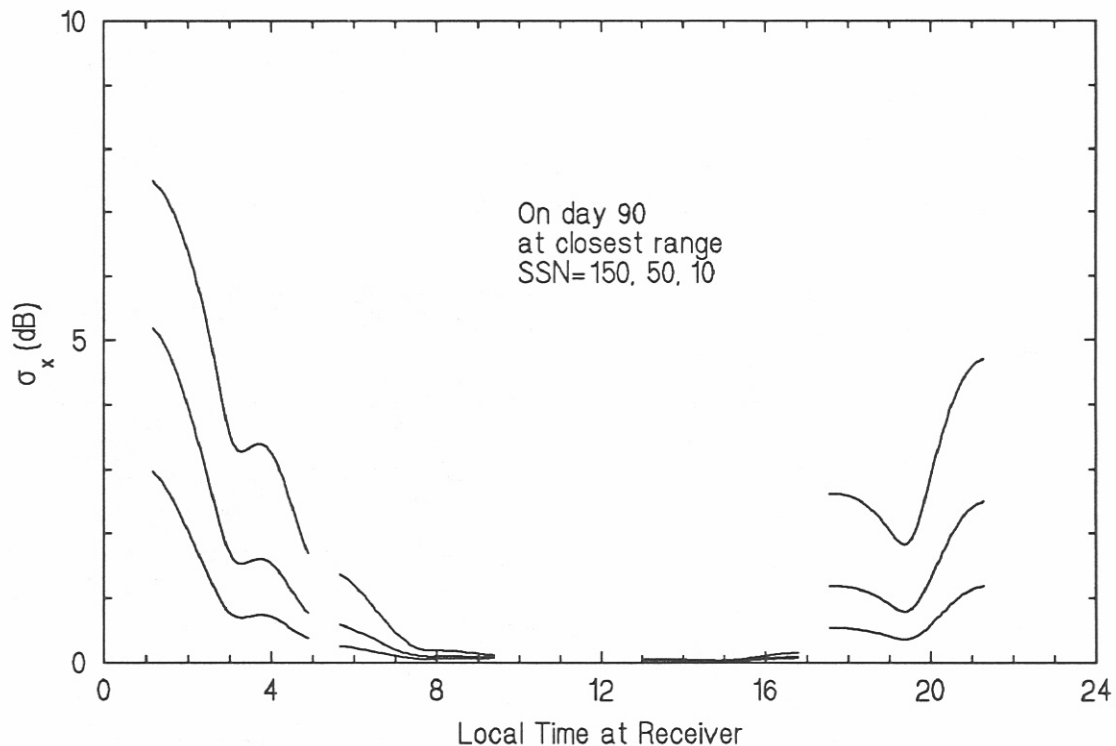Figure 6.   Average scintillation indices near Abidjan, Ivory Coast at 5° N, 4° W, during passes of TIROS as planned. The curves are drawn for three sunspot numbers.
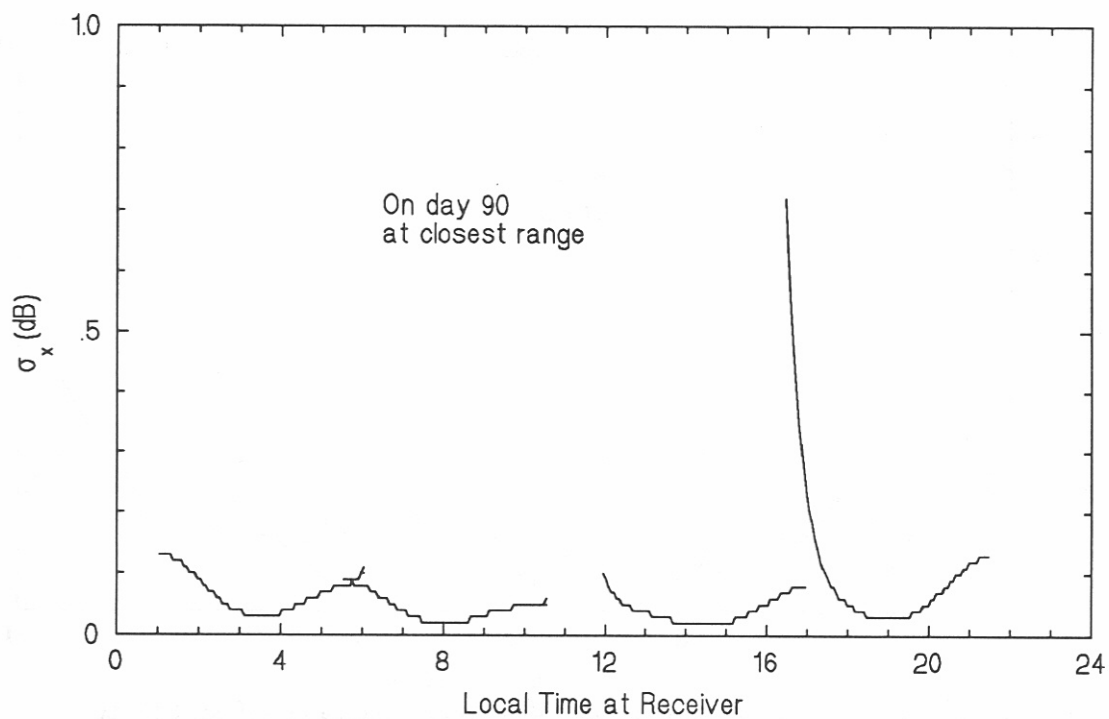
Figure 7. Average scintillation indices near Washington (USA) at 39⁰ N, 77⁰ W, during passes of TIROS. The deviations here are very small.
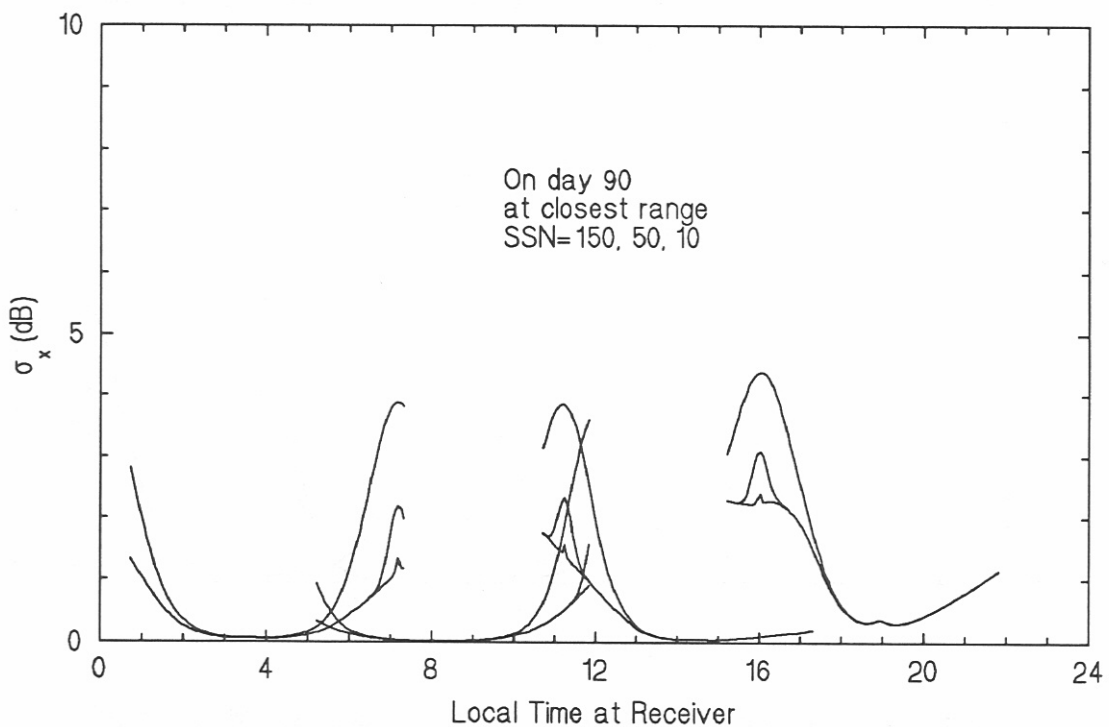
Figure 8. Average scintillation indices near Winnipeg, Canada at 50⁰ N, 97⁰ W, during passes of TIROS.

Figure 9. Average scintillation indices near Fairbanks, Alaska at 65^0 N, 148^0 W, during passes of TIROS. The receiver's northern location means it will see the satellites to the north at almost any time of the day.

Figure 10. Average scintillation indices near Helsinki, Finland at 60^0 N, 25^0 W, during passes of TIROS.

We should note here that in order to construct the results of the figures of this section, we were forced to use one of the original models for ion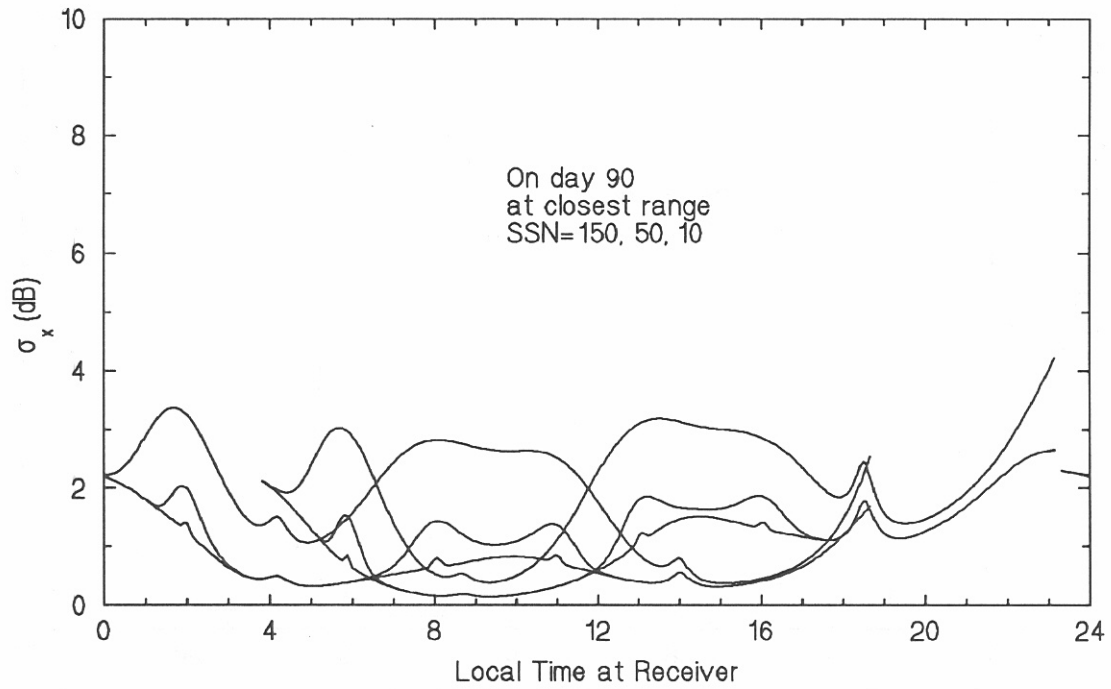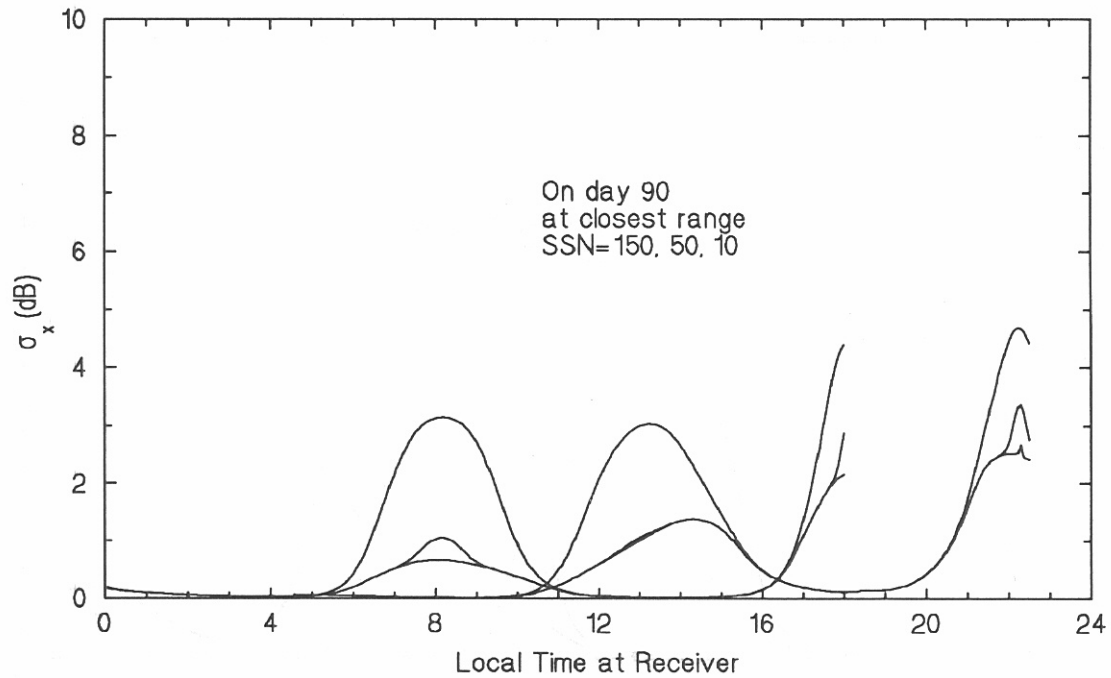ospheric scintillation. The model was suggested in 1973 by Fremouw and Rino [11] and implemented by Pope [12] in 1974. The latest version [13] of this same model will presumably give similar but distinctly different values. It is now becoming available for use, and in Figure 11 we compare the two versions, showing how they predict the average scintillation throughout one day at the equatorial site of Abidjan, Ivory Coast. Note in particular that the new version has limited the values when they approach conditions corresponding to Rayleigh fading. Note, too, the values obtained using the older version differ from values in Figure 5. Parameters for the receiver are the same but the transmitter on the satellite is at a different location.

To escape the harmful effects of scintillation one might propose a form of diversity reception. Unfortunately, the fields vary only slowly with time, space, frequency, or polarization. There is little "diversity action" and such proposals do not seem useful. Space diversity might serve, but the receiving antennas would need to be separated by 100 or 200 m.

The best way to avoid these effects seems to be to choose proper times of attempted reception. This is a fairly straightforward process in the equatorial regions where one could avoid the hours close to midnight. For the case under study, that means that the ascending and descending nodes should be carefully chosen. The present choices for APT, for example, are excellent ones.

4. EFFECTS OF RADIO NOISE ON THE WEATHER SATELLITE SYSTEM

The performance of a radio system is dependent on the received signal strength and the natural and man-made radio noise processes. In general, there are a number of noise processes to consider: the noise internally generated by the receiving system; natural noise (e.g., atmospheric, solar, and galactic); unintentionally radiated man-made noise; and intentionally radiated noise (e.g., interference). Typically, the noise processes depend on frequency, time, and location. Statistics related to a variety of natural and man-made sources have been compiled and published [e.g., 4.2, 4.3]. In this section, we review those noise sources that affect the broadcast of weather images at 137 MHZ and estimate (based on published statistics) the system noise temperature and the CNR for the high-end and low-end system receiving systems.

4.1 The Radio Noise Environment

Environmental noise is in general a nonstationary random process. Noise measurements are made over periods of time for which the process is stationary enough to obtain the required statistics (such as the rms voltage). Measured noise data commonly are given in terms of the external antenna noise figure F_a:

$$F_a = 10\log_{10}\frac{T_a}{T_0} = 10\log_{10}\frac{P_n}{kT_0 b} \ , \tag{8}$$
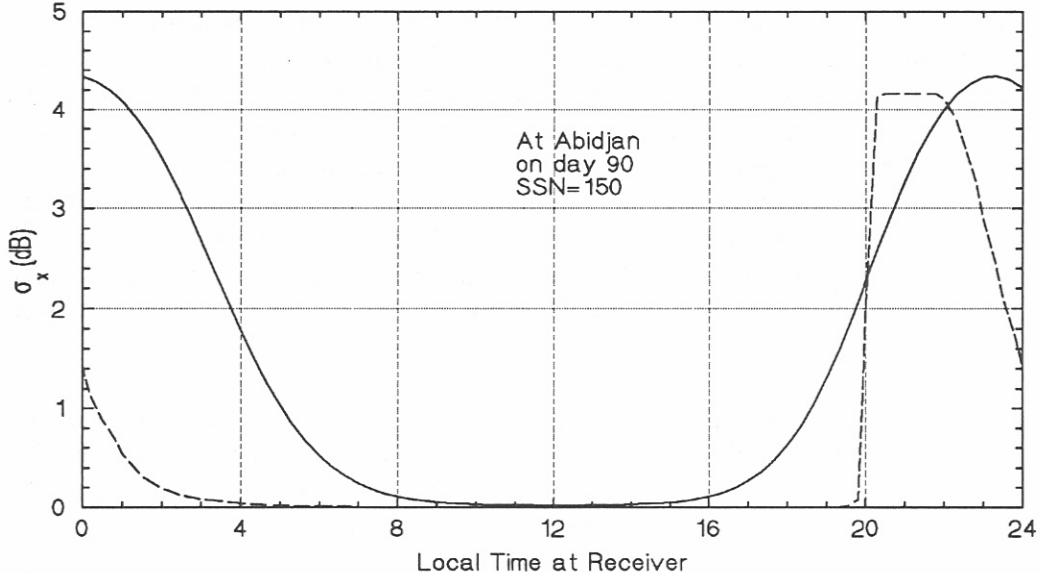
Figure 11. A comparison of two versions of our ionospheric scintillation model
near Abidjan, Ivory Coast. The newer version is given by the
dashed line, the older version is given by the solid line.

where p_n is the available noise power. Published statistics [14, 15, and 16] based on measurements provide information on the distribution of F_a (time and location variability) for natural and man-made noise environments.

The overall background natural radio noise from 1 Hz to 1 THz is shown in Figure 12 [14]. Note that around 137 MHZ, the important sources of natural radio noise are the sun and galactic noise. Figure 13 (a corrected figure from CCIR Report 670 [15]) shows the same results over a smaller frequency range (100 MHZ to 100 GHz). Here, the estimated median business-area man-made noise has been included. It is clear that in the frequency range of interest, man-made noise has a significant influence on the radio link.

The effects of the sun and galaxy can be estimated using the published statistics. As shown in the figures, the sun is a strong radio noise source. Since the sun has a diameter of about ½° and the receiving antennas have a relatively wide beamwidth, it is expected that the effect of the sun for the most part will not be important. This is particularly true for a Yagi-Uda receiving antenna since the sun will not always be within the main beam. The relationship between the noise temperature of the sun and the receiving antenna is given by the following expression:

$$T_{ant} = \frac{D}{4\pi} \int_{sources} T(\Omega)P(\Omega)d\Omega = DT_{sun}(\frac{\pi}{1440})^2, \qquad (9)$$

where D is the receiving antenna directivity and P is the antenna pattern. When a quiet sun
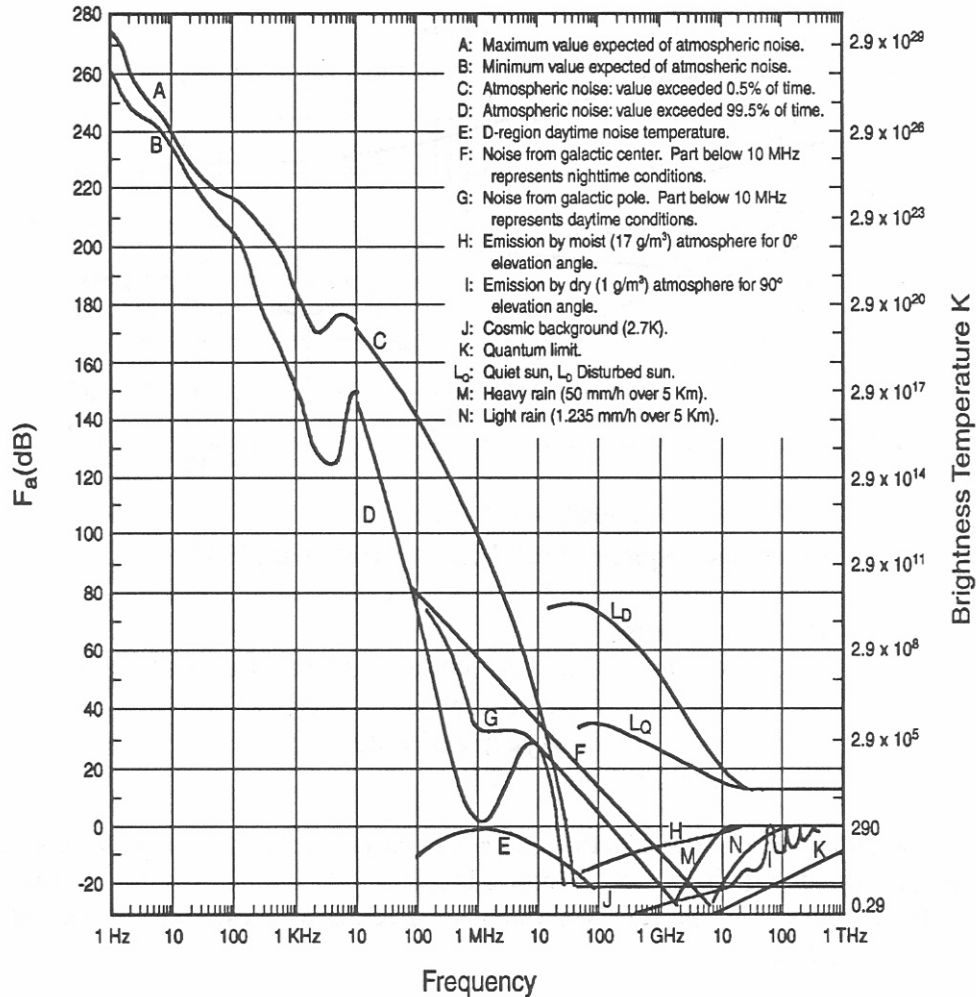
14

Figure 12. Natural radio noise, 1 Hz to 1 THz [14].

$(T \approx 1.5 \times 10^6$ K) is in view, the temperature of the Volute antenna is approximately 17 K and the temperature of the Yagi-Uda antenna is approximately 71 K. Figure 12, shows that the noise figure for a disturbed sun is roughly 30 dB greater than that for a quiet sun. It is expected that such extreme noise levels are sporadic and should not drive the system design process. These data indicate that a quiet sun will not have a significant effect on the radio link when compared to other environmental noise sources.

In Figure 13, there are two curves associated with galactic noise. The lower curve B is for an omnidirectional antenna, while the upper curve C is for an infinitely narrow beam aimed toward the galactic center. Maximum galactic noise for the weather satellite system should occur when the Yagi-Uda antenna is directed toward the galactic center. This maximum can be estimated using published radio sky data. CCIR Report 720-2 [16] provides maps of the brightness temperature of the radio sky at 408 MHz and an approximate expression for the frequency dependence of the noise. To obtain a more realistic value, published radio sky brightness temperatures at 150 MHz [17] were used to
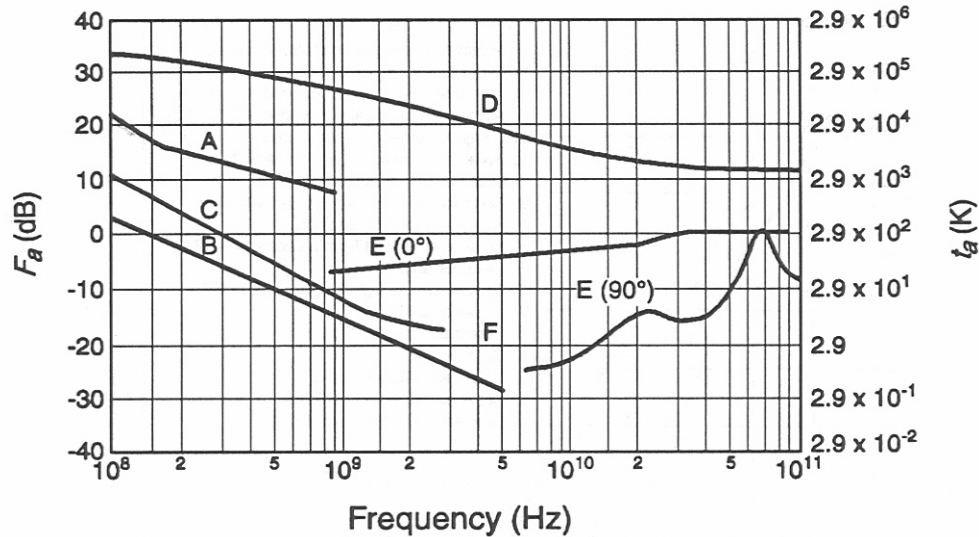
15

Figure 13. Fa versus frequency (100 MHZ to 100 GHz) [14].
              A. Estimated median business area man-made noise
              B. Galactic noise
              C. Galactic noise (galactic center - infinitely narrow beamwidth)
              D. Quiet sun (½ degree beamwidth directed at sun)
              E. Sky noise due to oxygen and water vapor
              F. Cosmic background 2.7 K

estimate the noise power when the galactic center is in view. Based on this data, it was found that the antenna temperature due to the galactic center is less than 600 K. We concluded that the galactic noise represented by curve C (560 K) should provide a reasonable estimate of the overall galactic noise power for this system.

The most significant single source of environmental noise is the contribution due to man-made sources. Figure 14 (from CCIR Report 258-5 [18]) gives a more detailed picture of man-made noise levels. In this figure, the median noise as a function of frequency, for four different environments (Table 1) is plotted along with galactic noise. As indicated previously, the noise figure is nonstationary and F_{am} represents the hourly median value.

The statistical distribution used in the following calculations is a composite Gaussian model that accounts for skewness. CCIR Report 258 provides upper (D_u) and lower (D_l) decile values for this distribution as a function of frequency and environment. Spaulding and Stewart [19] have analyzed the data used to obtain D_u and D_l for man-made noise and have found that it is appropriate to use D_u = 9.7 dB and D_l = 7 dB, independent of environmental category and frequency. This approach was used in the following calculations. The contribution due to galactic noise also is included in the cumulative distribution calculations. The galactic noise distribution was assumed to be Gaussian with $D_u = D_l = 2$ dB [19].

Examples of the calculated cumulative distributions of F_a for the sum of galactic and business, residential, rural, and quiet rural noise environments are shown in Figure 15. This figure gives the

16
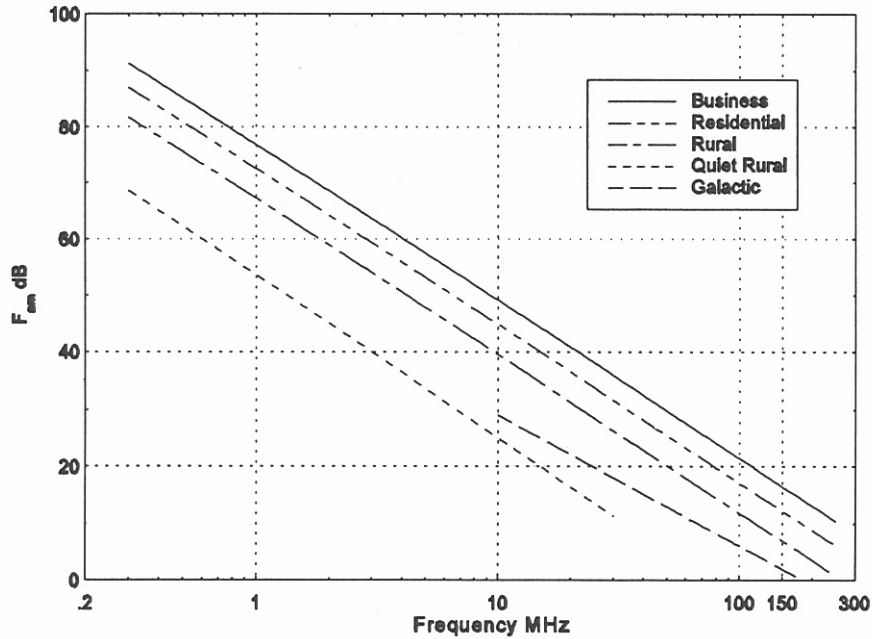
Figure 14. Median values of man-made and galactic noise.

probability (percent of an hour in this case) that F_a is exceeded. Note that the influence of galactic noise becomes more important for the larger probabilities.

Location variability is another important consideration. CCIR Report 258 gives the standard deviation of the median value with respect to location for the business, residential, and rural environments. As may be expected, location variability for the business environment is much larger than either the residential or rural environment. Location variability for the quiet rural environment should be small. The increased noise levels that may be expected for greater (than 50%) coverage are given in Table 2 (these quantities are added to F_a in Figure 15).

Table 1. CCIR Report 258 Definitions of Man-made Noise Environments

Environment	Characteristics
Business	Areas where predominant usage is for any type of business
Residential	Areas used predominantly for single or multiple family dwellings (at least 5 single family units per hectare); no large or busy highways
Rural	Areas where dwelling density is no more than 1 every 2 ha
Quiet Rural	No definition given

17
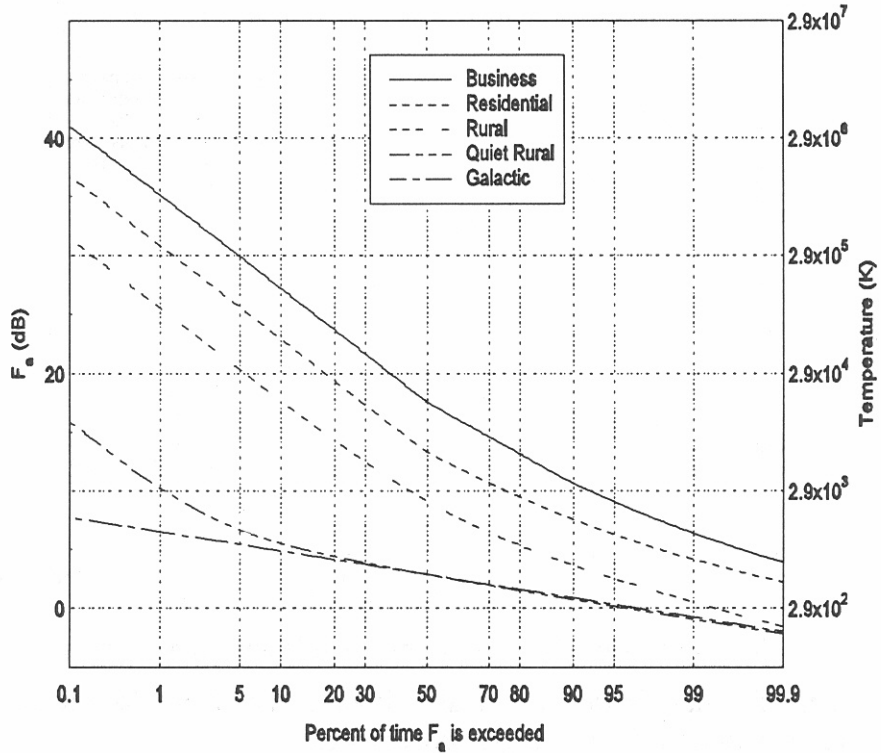
Figure 15. Distribution of F_a for man-made and galactic noise.

The measurements for the quiet rural noise environment are valid below 30 MHz as shown in Figure 14. In the calculations that follow, the curve is continued (slope of 28.6) to 137 MHz and the standard deviation recommended by Spaulding [19] is used to obtain the cumulative distribution shown in Figure 15. For exceedence levels of greater than 10%, the noise level in the so called quiet rural environment is due largely to galactic noise.

Table 2. Increased Noise Due to Location Variability

% locations	Business σ = 8.0 $\Delta F_a dB$	Residential σ = 2.7 $\Delta F_a dB$	Rural σ = 3.2 $\Delta F_a dB$
99	18.6	6.3	7.5
95	13.2	4.5	5.3
90	10.3	3.5	4.1
80	6.7	2.3	2.7
70	4.2	1.4	1.7
60	2.0	0.7	0.8

18

4.2 Modification of Noise Power for Proposed Receiving Antennas

Measurements of the man-made noise described above were made with a receiving antenna consisting of a short monopole above a perfectly conducting ground plane. Assuming that man-made noise is omnidirectional with respect to azimuth and arrives between 0° and 10° elevation, we estimated the gain in noise power (relative to the monopole) for the Volute and Yagi-Uda antennas described in Section 2 of this report. For the Volute antenna, the gain (for elevation angles of noise arrival) is roughly the same as for a short monopole antenna; hence, received noise power should be about the same as given in the previous section (e.g., Figure 15) irrespective of satellite elevation.

Since the Yagi-Uda antenna has a higher gain, the received noise power is significantly different than for the monopole antenna, and hence, will vary with elevation. Assuming the noise power arrives equally from all directions at elevations of less than 10°, and the antenna pattern is symmetric (crossed Yagi). The calculated relative antenna temperature for the Yagi-Uda and a monopole antennas over a perfect conductor is shown in Figure 16. Since the ground temperature is much smaller than the man-made noise temperature, it was not included in the calculation. For the purposes of this analysis, we were interested primarily in the relative gain for elevation angles of 90° and 5°. In terms of the link budget calculation, when the main beam elevation angle is at 90°, 5 dB should be subtracted from the noise; when the main beam elevation angle is at 5°, 5 dB should be added to the noise.

4.3 Receiving System Noise and Carrier-to-Noise Ratio

Using the information provided above, we estimated the noise power for man-made and galactic radio noise environments. Calculated values presented in this section are based on a time availability of
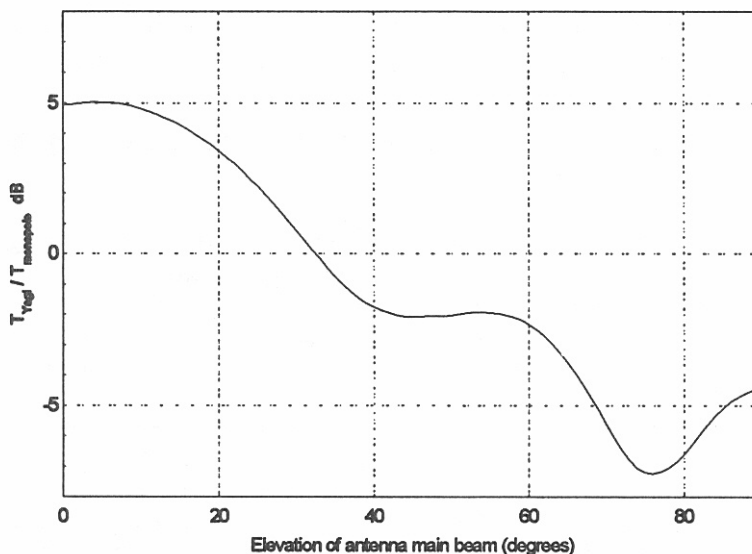

Figure 16. Variation of received noise as a function of elevation angle.

19

99.8% of the average year as required for the weather satellite system. Table 3 gives the noise figure (and temperature) exceeded 0.2% of the time for 50% of the locations. For coverage of more than 50% of locations, the appropriate ΔF_a from Table 2 should be added.

The system noise power for the high-end system (receiver noise figure of 1 dB) and the low-end system (receiver noise figure of 6 dB) are given in Section 2 of this report. Note that the low-end receiver contributes about 1,500 K to the system temperature. For practical considerations (i.e., changes in noise power of more than a few tenths of a dB), the receiver noise figure only matters when the Yagi-Uda antenna is in a quiet rural environment and at elevations of around 90°. In this case, the temperature increases to 4,041 K (or a 2-dB increase in the system noise figure). It should be noted that an observation elevation of 90° is a relatively infrequent occurrence. Based on the required time availability, there is no practical distinction between the high-end receiver and the low-end receiver, particularly if greater than 50% location availability is desired.

Table 4 gives the calculated CNR exceeded for the two receiving antennas (for areas unaffected by ionospheric scintillation) for 50% of the locations 99.8% of the time. The bandwidth is 72 kHz and the receiver noise figure is 6 dB, which as indicated above has little effect on CNR. Details of the link calculation used to obtain the results shown in Table 4 are provided in Appendix A. Table 4 includes results for the CNR exceeded 90% of the time. Plots of the cumulative distributions (% of time that a given CNR is exceeded) for the various cases shown in Table 4 also are given in Appendix A

4.5 Issues Pertaining to Man-made Noise Statistics

The man-made noise statistics presented are largely based on measurements that were made more than twenty years ago in North America [20]. Since that time, the number of cars has increased; however, there have been improvements in the suppression of noise from automobile ignition systems (a major contributor to man-made noise in urban areas) and one may predict that noise levels

Table 3. Noise Figure/Temperature for the System Receiving Antennas

Environment	Volute Antenna		Yagi-Uda Antenna 90° Elevation		Yagi-Uda Antenna 5° Elevation	
	F_adB	T_aK	F_adB	T_aK	F_adB	T_aK
Business	39.4	2.5×10^6	34.9	9.0×10^5	44.4	8.0×10^6
Residential	35.1	9.4×10^5	30.1	3.0×10^5	40.1	3.0×10^6
Rural	29.8	2.8×10^5	24.8	8.8×10^4	34.8	8.8×10^5
Quiet Rural	14.3	7.8×10^3	9.3	2.5×10^3	18.3	2.0×10^4

in business and residential environments has decreased. In a 1995 paper, Spaulding [14] reviewed more recent measurements and trend analysis presented by various researchers. In this paper, he discusses the likelihood that noise levels have dropped by 10-20 dB and concludes that "at 100 MHz in the 1970's time-frame, F_a was on the order of 20 dB but now is probably approximately 20 dB less." This conclusion, however is not based on a comprehensive set of noise measurements as would be necessary to update the previous survey described in reference [20].

While the improvements in automobile ignition systems have affected the noise levels in business and residential environments, the contribution due to power transmission and distribution lines, where the noise contribution at 100 MHz is due to gap discharge and corona, has probably not decreased with time. Figure 17 shows F_a under and a 1/4 mile from a 115-kV line in rural Wyoming. Note that the noise measured a 1/4 mile from the power line parallels that predicted for a rural environment. If power and distribution lines are the primary noise source in rural environments, rural man-made noise is not expected to have decreased. Also, one would not expect noise in an urban environment to be less (than rural), as would be the case with a 20-dB reduction in F_a.

The results presented in this section are applicable to North America; the validity of extension to other parts of the world cannot be determined precisely. CCIR Report 258 describes VHF measurements made in business and residential areas of the United Kingdom where the noise powers were found to be some 10 dB below the results in Figure 4.3. The differences are attributed to differences in patterns of utilization of electrical and mechanical appliances, regulations of interference, etc. The report also states that due to such differences, the noise statistics should be used with caution. It is interesting to note that if an overall 10-dB reduction in urban noise can be justified, the man-made noise environments near 100 MHz would be bounded by what are now classified as rural (worst) and quiet rural (best) environments.

In summary, it is likely that there are business (and/or residential) environments with noise levels 10 dB or more below accepted published values. Although applying a 10-dB reduction to published

Table 4. CNR (dB) for the Volute and Yagi-Uda Antennas at Maximum (90°) and Minimum
(13° and 5°, respectively) Elevation Angles

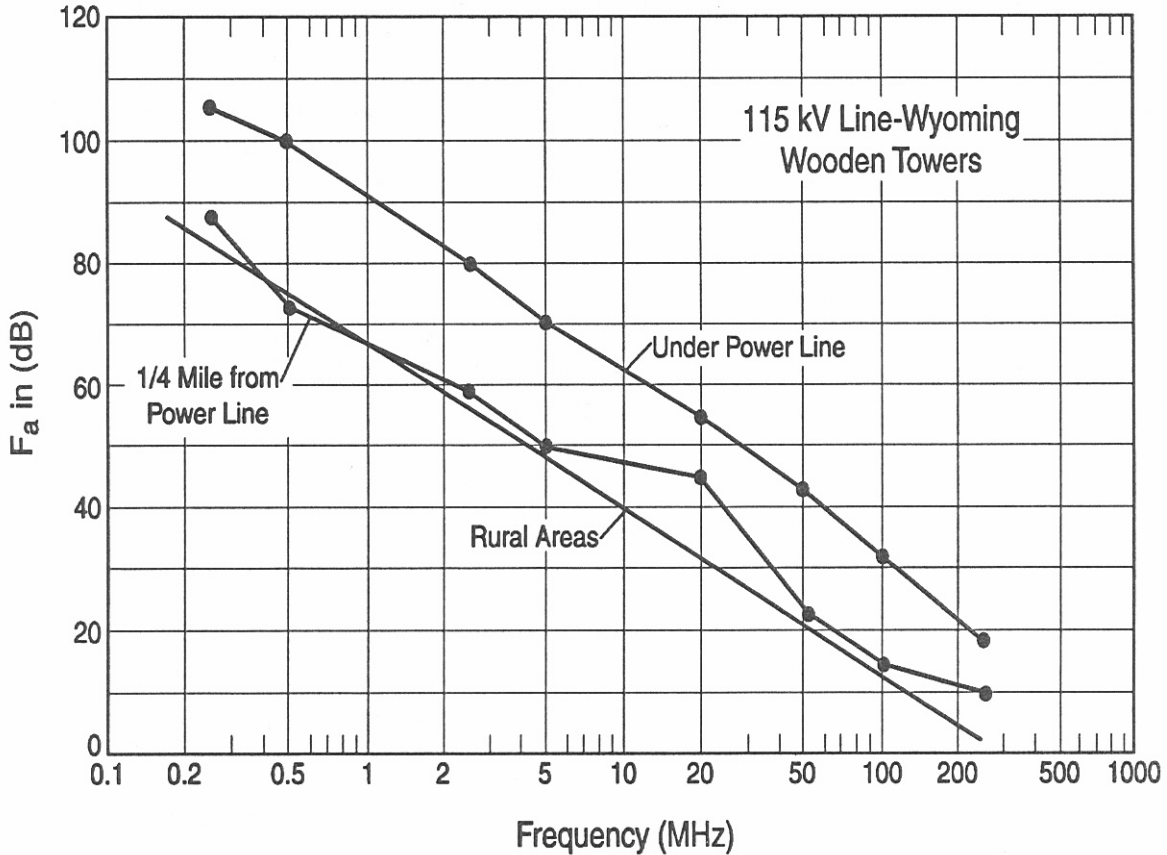| Environment	5-W Transmitter				5-W Transmitter			
	Volute		Yagi-Uda		Volute		Yagi-Uda	
	90°	13°	90°	5°	90°	13°	90°	5°
Business	-5.8	-20.8	5.7	-18.7	-1.0	-16.1	10.5	-14.0
Residential	-1.5	-16.5	10.0	-14.4	3.3	-11.8	14.8	-9.7
Rural	3.8	-11.2	15.3	-9.1	8.6	-6.5	20.0	-4.4
Quiet Rural	18.6	3.5	30.3	6.3	23.3	8.3	35.1	11.1

Figure 17. Power line noise measurements near a 115-kV line in rural Wyoming [20].

man-made noise statistics for business/residential environments may appear to be reasonable, the validity of doing so as a general rule is untested at the present time.

5. CARRIER-TO-NOISE RATIO REQUIREMENTS FOR LRPT LINK

This section describes how CNR requirements vary for different signal designs. Signal design in this context refers to the link modulation, demodulation, and error-correction coding. First, the signal designs are described; next calculations for the required CNR for each signal design are presented; and finally, signal design factors other than required CNR that may impact LRPT link performance are discussed. Appendix B gives equations used for computations contained in this section.

5.1 Signal Design Description

The signal design includes modulation, demodulation, and error correction. In this subsection, signal designs that were analyzed are described.

5.1.1 Modulation/Demodulation

Binary phase-shift keying (BPSK) and quadrature phase-shift keying (QPSK) modulation are considered in this report. Without differential source encoding, BPSK and QPSK demodulation require coherent detection and a method such as unique word insertion to resolve phase ambiguities at the receiver. If differential source encoding is used, phase ambiguities are resolved without unique word insertion; however performance is degraded. Examples of binary and quadrature differential-encoding algorithms are available in [21, 22].

Differentially encoded BPSK or QPSK can be detected coherently or differentially. If they are detected coherently, they are called differentially encoded binary phase-shift keying (DEBPSK) or differentially encoded quadrature phase-shift keying (DEQPSK) demodulation. The coherently detected symbols are sampled, mapped into bits, and differentially decoded.

Differential BPSK (DBPSK) and differential QPSK (DQPSK) demodulation use differential detection. DBPSK detection is accomplished by multiplying the current symbol by the previous symbol. DQPSK detection is accomplished by multiplying the current symbol by the previous symbol in both I and Q channels. The differentially detected symbols are sampled and mapped into bits. There is no need to differentially decode the bits.

5.1.2 Error-Correction Coding

The Reed Solomon (RS), convolutional (CV), and concatenated (CC) coding error-correction methods [22] used in this study are derived from [23, 24]. Key parameters for the codes are rate and distance. The rate is the ratio of the number of codeword symbols n to information symbols k. The distance is a measure of the difference between codewords.

RS $(n = 255, k = 223)$ code has a 7/8 rate and 32 symbol distance and is used in all proposed signal designs [25, 26]. The 32 redundancy symbols allow correction of up to 16 of the 255 codeword symbols. A symbol for the RS (255, 223) code is 8 bits or 1 byte long. The 223 information bytes transmitted can be used "as is" or may be corrected by using the 32 redundancy bytes. RS codes are known for their error-burst-correction capabilities and require codeword synchronization.

CC coding uses an inner CV code with a outer RS code [27, 28, 29, 30]. The performance of a CC can be calculated by computing the probability of error at the output of the CV decoder and then using this result as the input probability of error to the RS decoder.

The $(k = 1, n = 2, K = 7)$ CV code generates 2 coded bits from one information bit for a code rate of~ with a minimum free distance of 10. The K is the code's constraint length and for the (1, 2, 7) CV code represents the number of shift register bits used to generate the code. The Viterbi algorithm decodes the CV -encoded bits.

An RS interleaver usually is placed between the CV decoder and the RS decoder to minimize the effect of error bursts produced by the CV decoder on the RS decoder. Error burst length for the (1, 2, 7) CV code is defined as a string of bits that starts and stops with a gap of at least six correct bits. The error bursts are caused by insufficient received CNR and node synchronization. Node synchronization occurs when the beginning of the convolution encoder n-tuples is known. If the beginning is not known, the node is not synchronized and BER approaches 0.5. The process of node synchronization may take hundreds of symbols.

5.1.3 Signal Designs

Table 5 lists the signal designs that are capable of providing the specified data rate with the same 99% bandwidth. QPSK schemes have CC coding while BPSK schemes use only RS coding.

Table 5. Possible Signal Designs for the LRPT Link

Modulation	Coding
BPSK	RS
DEBPSK	RS
DBPSK	RS
QPSK	CC
DEQPSK	CC
DQPSK	CC

5.2 Required Carrier-to-Noise Ratios

The required CNR is the symbol energy-to-noise ratio (Es/No) plus the modulation and demodulation losses for a given signal design:

$$CNR_{required} = Es / No + L_{m/d} \tag{10}$$

Link margins are computed by subtracting the required CNR from the received CNR (link margins are given in Appendix A).

The LRPT link requires a data rate of 72 kbps at the input to the RS decoder. This data rate includes all packet overhead. A BER of 10^{-6} is assumed to be sufficient for the image compression algorithm to deliver the necessary image quality. Rectangular pulse shaping is assumed. Results are valid for Gaussian noise only.

24

5.2.1 Modulation and Demodulation Losses

To determine the required CNR, the modulation and demodulation losses must be estimated. These losses include imperfections in 1) transmitter and receiver filtering, 2) carrier recovery, 3) clock recovery, 4) I/Q amplitude balance, 5) I/Q time symmetry, 6) oscillator phase noise, and 7) power amplifier linearities. For this study, modulation and demodulation losses were estimated to be 2.0 dB for BPSK signal designs [31] and 3.0 dB for QPSK signal designs [32].

5.2.2 Symbol Energy-to-Noise Ratio

All signal designs include RS coding. Figure 18 shows the output bit error rate of the RS code as a function of input BER. The input bits are assumed to be degraded by an additive white Gaussian noise (AWGN) channel.

In Figure 18, a BER of 0.0025 is needed at the input of the RS decoder to produce a BER of 10^{-6} at the output of the RS decoder. Figure 19 shows the BER performance for all BPSK demodulators. The required Es/No is determined by the intersection of each curve with the 0.0025 BER point. BPSK, DEBPSK, and DBPSK require an Es/No of 5.8, 6.5, and 7.2 dB, respectively.

For QPSK modulation, we determined the Es/No required for the CV decoder to maintain a BER of 0.0025 at the input of the RS decoder. Figure 20 shows the performance of QPSK with a (1, 2, 7) CV code. Figure 21 shows the performance of DQPSK with a (1, 2, 7) CV code. A Viterbi algorithm path memory length of 32 and no quantization of the input samples was assumed.

The required Es/No for QPSK + CC and DEQPSK + CC can be read directly from Figure 20. QPSK + CC needs 2.6 dB to produce a BER of 0.0025 at the input of the RS decoder. DEQPSK + CC needs 2.8 dB to produce a BER of 0.00125 at the output of the CV decoder. The BER of DEQPSK is doubled to 0.0025 by the differential decoder prior to the input of the RS decoder. Figure 21 shows that the required Es/No for DQPSK + CC is 5.2 dB.

5.2.3 Results

Table 6 summarizes the Es/No, coding gain, and required CNR needed for each signal design. The coding gain is the difference between 10.5 dB (the Es/No needed for uncoded BPSK and BER of 10^{-6}) and the Es/No needed for that signal design. The highlighted rows indicate the two signal designs used for link margin computations.
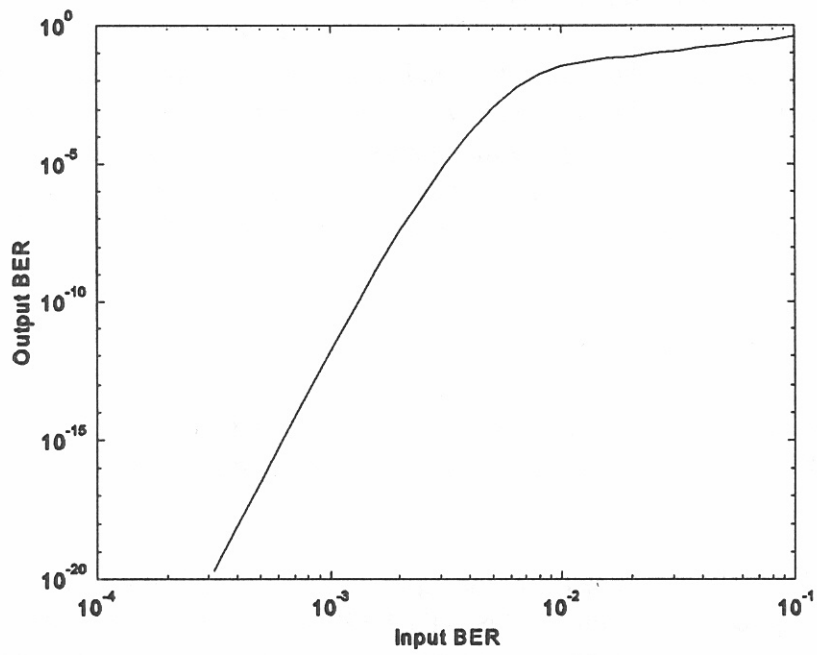
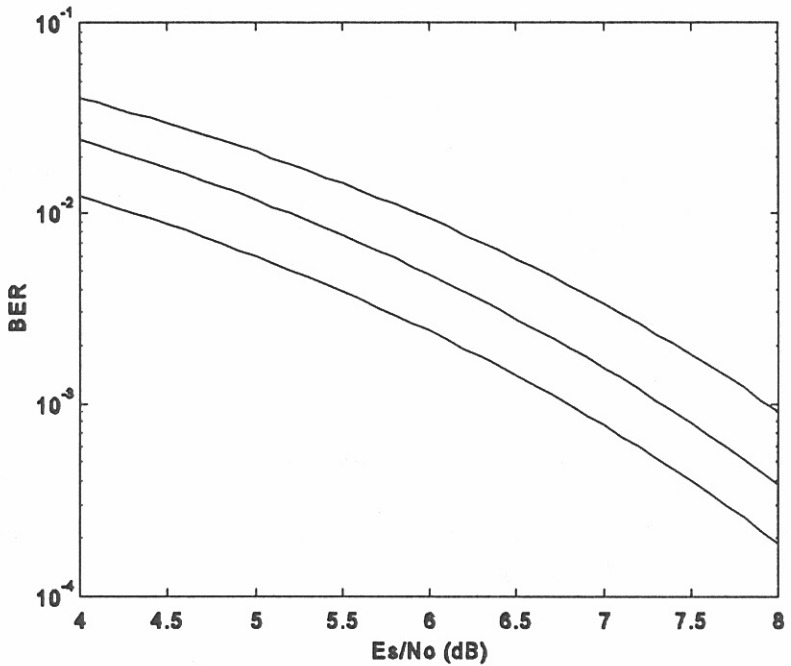Figure 18. Reed Solomon (255, 223) input to output BER performance.

Figure 19. BER for BPSK (lower curve), DEBPSK (middle curve), and DBPSK (upper curve).
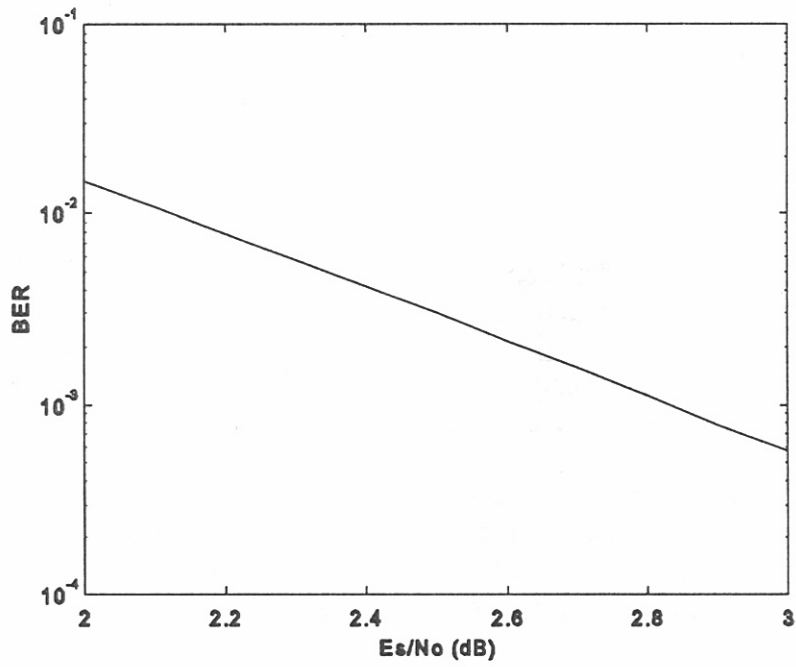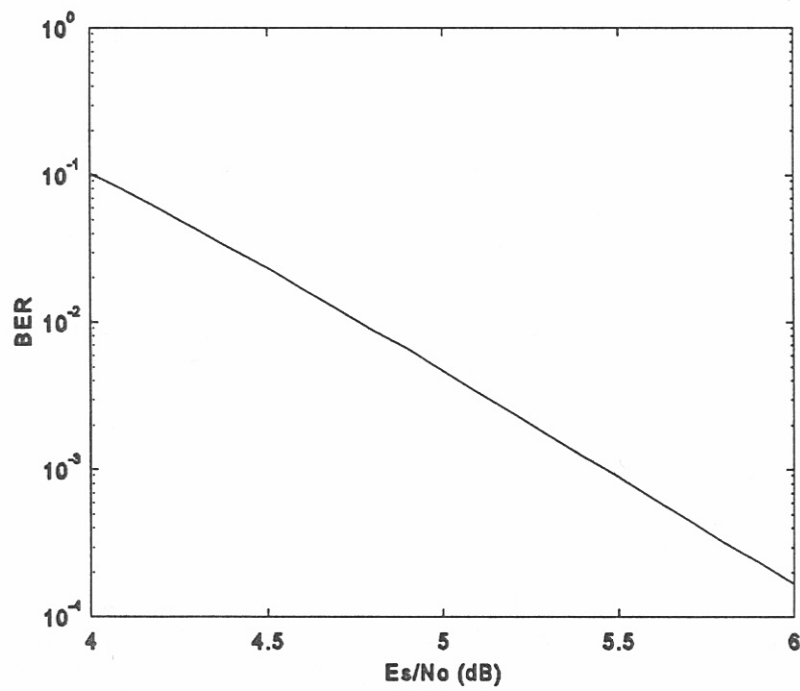
Figure 20. BER for (1,2,7) CV-coded QPSK.

Figure 21. BER for (1, 2, 7) CV coded DQPSK.

5.3 Other Signal Design Considerations

Other demodulation issues, including 1) carrier recovery, 2) symbol timing, 3) non-Gaussian noise, and 4) ionospheric scintillation are discussed in this section.

5.3.1 Carrier Recovery

Carrier frequency tracking is required for all of the signal designs since a Doppler shift due to the satellite's movement causes the center frequency to shift. BPSK, DEBPSK, QPSK, and DEQPSK are coherent detection methods that require carrier phase tracking also. Phase jitter caused by imperfect carrier phase tracking increases the BER [33]. Additional energy, included in the demodulator losses, is needed to overcome excessive phase jitter.

All of the signal designs are assumed to be transmitted as double sideband suppressed carrier channel waveforms. A nonlinearity followed by a narrowband filter (or phase-locked loop) is often used to generate a harmonic of the carrier frequency for carrier recovery. BPSK requires a second order nonlinearity while QPSK requires a fourth order nonlinearity [34]. Figure 22 shows the rms phase jitter in radians as a function of input Es/No.

Figure 22 shows that QPSK phase jitter is greater than BPSK for a fixed narrowband filter bandwidth *B*. Table 7 shows the required Es/No for each demodulator and its associated rms phase jitter. Phase jitter for QPSK signal designs is an order of magnitude larger than BPSK signal designs.

5.3.2 Symbol Timing

Symbol-timing recovery is required for all the signal designs. Timing jitter caused by imperfect symbol timing recovery increases the BER [33]. Additional energy, included in the demodulator losses, is needed to overcome excessive timing jitter.

Table 6. Signal Design Results (BER 10^{-6}, 72 kbps, shading represents designs used in Appendix A)

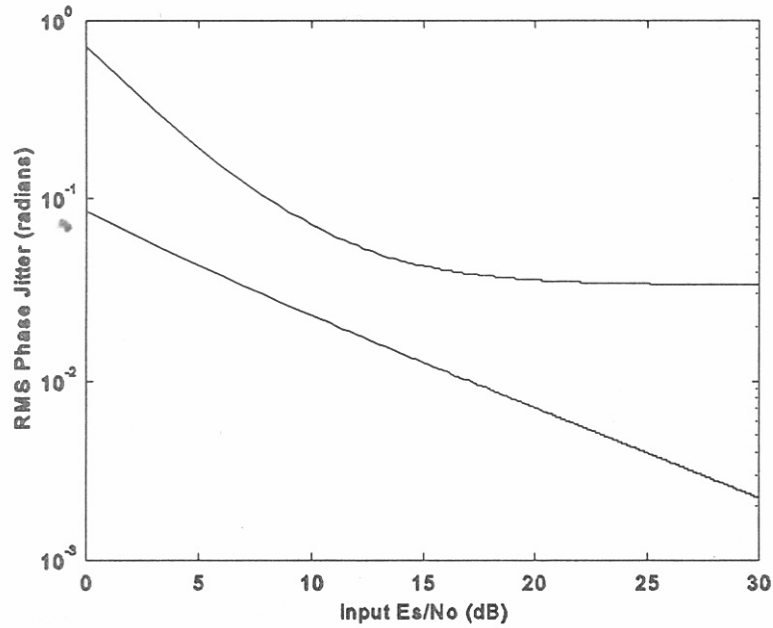| Signal Design	Es/No (dB)	Required CNR (dB)	Coding Gain (dB)
BPSK + RS	5.8	7.8	4.7
DEBPSK + RS	6.5	8.5	4.0
DBPSK + RS	7.2	9.2	3.3
QPSK + CC	2.6	5.6	7.9
DEQPSK + CC	2.8	5.8	7.7
DQPSK + CC	5.2	8.2	5.3

Figure 22. Carrier phase recovery for BPSK (lower curve), and
QPSK (upper curve) when BT = 0.01.

Symbol timing recovery commonly is implemented with a delay and multiply circuit followed by a narrowband filter, with bandwidth *B,* tuned to the symbol rate. In QPSK signal designs the delay and multiply circuit is performed in I and Q channels, which are then combined to form the timing waveform [35]. Figure 23 shows the rms timing jitter in radians as a function of input Es/No.

Table 8 shows the Es/No for each signal design and its associated rms timing jitter. The table shows that QPSK symbol timing recovery performance is similar to BPSK.

Table 7. Signal Design RMS Phase Jitter for BT = 0.01 (shading represents designs used in Appendix A)

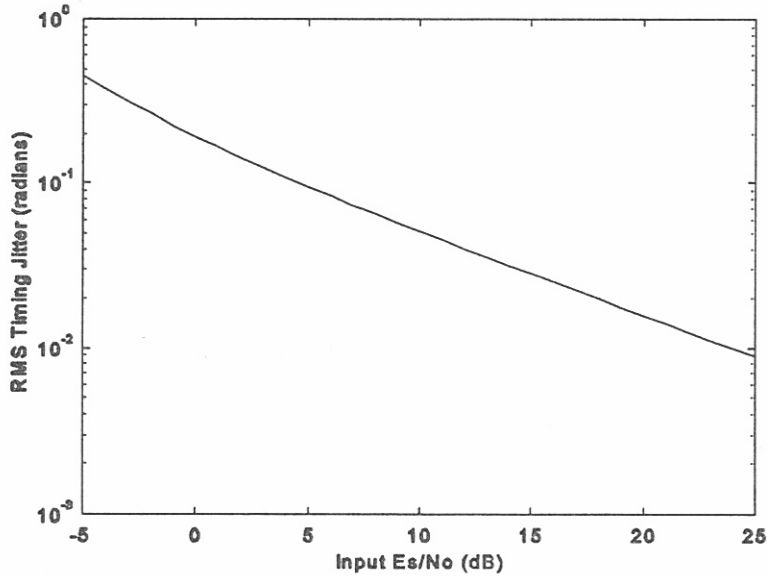| Signal Design	Es/No (dB)	RMS Phase Jitter (radians)
BPSK + RS	5.8	0.040
DEBPSK + RS	6.5	0.035
QPSK + CC	2.6	0.30
DEQPSK + CC	2.8	0.30

Figure 23. Symbol timing recovery for BPSK and QPSK when BT = 0.01.

5.3.3 Non-Gaussian Noise

All calculations in this section assume additive white Gaussian noise. It should be noted that man-made noise is typically non-Gaussian. Simulation is required to assess the impact of man-made noise on these signal designs.

5.3.4 Ionospheric Scintillation

Ionospheric scintillation causes the received signal power to vary over time. Interleavers are used to decrease the probability that adjacent symbols experience the same power fade. The performance of CV codes operating in a Rician-fading channel with and without interleaving has been well documented [36, 37]. However, interleaving is optimal when $B_dTI = 0.01$, where B_d is a measure of the channel's fading rate, T is the symbol period, and I is the interleaving depth. Improvement in performance is possible with $B_dTI < 0.01$. Relaxing this constraint decreases interleaver memory and delay. Simulation is required to assess the impact of interleaving on these signal designs.

6. SUMMARY AND CONCLUSIONS

For the purposes of this study, two archetypal E/S receivers were defined: a low-end system and a high-end system. The high-end system consists of a high-gain-tracking antenna combined with a high-quality receiver having a noise figure of 1 dB. The low-end system consists of an "omnidirectional" antenna combined with an average quality receiver having a noise figure of 6 dB.

30

Table 8. Signal Design RMS Timing Jitter for BT = 0.01 (shading represents designs used in
Appendix A)

Signal Design	Detection Es/No (dB)	RMS Timing Jitter (radians)
BPSK + RS	5.8	0.09
DEBPSK + RS	6.5	0.08
DBPSK + RS	7.2	0.07
QPSK + CC	2.6	0.12
DEQPSK + CC	2.8	0.12
DQPSK + CC	5.2	0.09

The typical high-end antenna is a crossed Yagi-Uda with a gain of about 10 dB. Both antennas are circularly polarized. Propagation studies at 137 MHz conducted by ITS conclude that scintillation effects may be detrimental in the equatorial and high-latitude regions. In the equatorial regions, scintillation occurs typically in the late night to early morning hours. In the high-latitude regions, scintillation is independent of time except near the polar extremities where scintillation is strongest at night. Midlatitude regions, including the United States, should not be affected significantly except possibly during fierce magnetic storms.

The normalized variation in received signal power (scintillation index) was calculated from the Ionospheric Scintillation Model developed for the U.S. Air Force by Fremouw and Rino [11]. Our analysis shows that scintillation fading of 10 dB or more can occur during peak solar activity in the high latitudes or in the vicinity of the magnetic equator. It is expected that such occurrences are somewhat rare over the 11-year solar cycle. Fades exceeding 3 dB have an average duration of 1 s.

Link margin calculations for the results presented are based on the 1990 CCIR Report "Man-made radio noise" (Report 258-5) that is based on work by Spaulding and Stewart over 20 years ago [19]. More recently, Spaulding estimated that man-made noise at 100 MHz in business environments had decreased 10-20 dB from the 20-dB level in the 1970's [14]. We are recommending that measurements be made in the representative environments to determine if noise levels have in fact changed significantly.

A variety of modems and channel-coding techniques ("signal designs") were analyzed to determine the CNR ratio necessary to meet the required 10^{-6} BER for LRPT image transmission at 72 kbps. The modems analyzed were 2 and 4-ary phase-shift keyed with and without differential detection or

decoding. These modems were combined in the analysis with Reed Solomon or concatenated coding. All performance calculations and link margins are for additive white Gaussian noise without multipath. The effects of non-Gaussian man-made noise should be investigated.

Tables 9 and 10 give the link margins as a function of noise environment, time availability (99.8% and 99%), maximum (13° elevation) and minimum (90° elevation) propagation path length, and two modulation/coding schemes. Shaded areas indicate that the minimum 1-dB link margin is satisfied. These tables show that increasing the transmitter power from 5 W to 15 W does not have a significant effect on coverage. We also determined that if time availability requirements are relaxed, coverage is increased significantly.

Table 9.   Link Margins in dB for Low-End System, 99.8% Time Availability and 5-W Transmitter (Dark shading meets 1-dB margin with 5-W transmitter. Light shading extends coverage for a 15-W transmitter.)

	13° Elevation		90° Elevation	
	DEBPSK+RS	**DEQPSK+CC**	**DEBPSK+RS**	**DEQPSK+CC**
Business	-29	-26	-14	-12
Residential	-25	-22	-10	-7
Rural	-19	-17	-5	-2
Quiet Rural	-5	-2	+10	+13

Table 10.   Link Margins in dB for Low-End System, 90% Time Availability and 5-W Transmitter (Dark shading meets 1-dB margin with 5-W transmitter. Light shading extends coverage for a 15-W transmitter.)

	13° Elevation		90° Elevation	
	DEBPSK+RS	**DEQPSK+CC**	**DEBPSK+RS**	**DEQPSK+CC**
Business	-17	-15	-2	+1
Residential	-13	-10	+2	+5
Rural	-8	-5	+7	+10
Quiet Rural	+1	+3	+16	+18

7. REFERENCES

[1]   T. Pratt and C.W. Bostian, Ch. 4 of *Satellite Communications.* New York, NY: John Wiley & Sons, 1986.

[2]   Martin Marietta, "Satellite to Ground Interface (NOAA-K, L, M)," document code ident. no. 18713, IS3278200, obtained from NOAA, 1995.

[3]   R.J. Summers, "Educator's guide for building and operating environmental satellite receiving stations," NOAA Technical Report NESDIS 44, 1989.

[4]   C.A. Chen and D.K. Cheng, "Optimum element lengths for Yagi-Uda arrays," *IEEE Trans. Antenna Propagat.,* vol. 23, no. 1, pp. 8-15, 1975.

[5]   RCA, "Performance Specification- VHF Real-Time Antenna (VRA)," document code ident. no. 49671, PS-2280287, sheet 8, Jun. 1995

[6]   L. Boithias and D. Beesen, Ch. 4 of *Radio Wave Propagation,* New York, NY: McGraw-Hill Book Company, 1987.

[7]   T. Sullivan and S. Klein, "NOAA OPQ satellite HRPT and LRPT data handling and transmission systems," prepared for the National Aeronautics and Space Administration Goddard Space Flight Center, Code 970.1, Oct., 1991.

[8]   M.P .M. Hall, *Effects of the Troposphere on Radio Communication,* IEE Electromagnetic Wave Series, London, 1979.

[9]   B.R Bean and E.I. Dutton "Radio meteorology," *NBS Monograph* 92, 1966.

[10]   W.L. Flock, "Propagation effects on satellite systems at frequencies below 10 GHz," NASA Ref. Pub. 1108(02), 1987.

[11]   E.J. Fremouw and C.L. Rino, "An empirical model for average F-layer scintillation at VHF/UHF," *Radio Science* vol. 8, no.3, pp. 213-222, 1973.

[12]   J.H. Pope, "Global scintillation model," NOAA Tech. Report ERL308-SEL30, 1974.

[13]   J.A. Secan, R.M. Bussey, E.J. Fremouw, and S. Basu "An improved model of equatorial scintillation," *Radio Science,* vol. 30, no. 3, pp. 607-617, May-June 1995.

[14]   A.D. Spaulding, "The roadway natural and man-made noise environment," *IVHS Journal,* vol. 2(2), pp. 175-211, 1995.

[15] Recommendations and Reports of the CCIR, "'Worldwide minimum external noise levels, 0.1 Hz to 100 GHz," XVth Plenary Assembly, Report 670, 1990.

[16] Recommendations and Reports of the CCIR, "Radio emission from natural sources in the frequency range above about 50 MHz ," XVth Plenary Assembly, Report 720-2, 1986.

[17] T.L. Landecker and R. Wielenbinski, "The galactic metre wave radiation," *Aust. J. Phys. Astrophys. Suppl.,* no. 16, pp. 1-30, 1970.

[18] Recommendations and Reports of the CCIR, "Man-made radio noise," XVIIth Plenary Assembly, Report 258-5, 1990.

[19] A.D. Spaulding and F.G. Stewart, "An updated noise model for use in IONCAP," NTIA Report 87-212, Jan. 1987.

[20] A.D. Spaulding and R.T. Disney, "Man-made noise: Part I," Office of Telecommunications Report 74-38, Jun. 1974.

[21] K. Feher, *Digital Communications,* Englewood Cliffs, NJ: Prentice Hall, pp. 138-140 and 169-171, 1981.

[22] E.R. Berlekamp, "The technology of error correction codes," *Proc. IEEE,* vol. 68, no. 5, pp. 564-593, 1980.

[23] Consultive Committee for Space Data Systems, "Telemetry: Summary of concept and rational," CCSDS 100.0-G-1 Green Book, pp. 3-20, Dec. 1987.

[24] Consultive Committee for Space Data Systems, "Telemetry channel coding," CCSDS 101.0-B-3, Blue Book, May 1992.

[25] W.E. Toms, "An application of Reed Solomon codes to a satellite TDMA system," in *Proc. MILCOM 1986*, Monterey, CA, pp. 12.5.1-12.5.8, Oct. 1986.

[26] J.G. Proakis, *Digital Communications 3rd Edition,* New York, NY: McGraw Hill, pp. 464-466 and 470-511.

[27] E.R Belekamp, "The applications of error control to communications," *IEEE Communications Magazine,* vol. 25, no. 4, pp 44-57, 1987.

[28] H.F. Roefs, "Concatenated coding in a spacecraft to ground telemetry channel: Performance," in *Proc. 1981 Internat. Conf. Comm.,* pp. 2.6.1-2.6.5, 1981.

[29]   K.Y. Liu, "Recent results on the use of concatenated Reed Solomon/Viterbi channel coding and data compression for space communications," *IEEE Trans. Comm.,* vol COM-32, no. 5, pp. 518-523, 1984.

[30]   A.J. Viterbi, "Convolutional codes and their performance in communication systems," *IEEE Trans. Comm.,* vol. COM-19, no. 10, pp. 751, 1971.

[31]   Atlantic Research Center, "NOAA OPQ satellite HRPT and LRPT data handling and transmission systems," report prepared for the National Aeronautics and Space Administration, Goddard Space Flight Center, Code 970.1, Oct. 4, 1991.

[32]   S. Di Girolamo, "Low rate picture transmission (LRPT) for METOP platform," Alenia Spazio, MO-TN-ALS-LR-1029, issue 2, Nov. 30, 1995.

[33]   V.I. Stiffler, *Theory of Synchronous Communications,* Englewood, Cliffs, NJ: Prentice Hall, pp. 268-277, 1971.

[34]   L.E. Franks, "Carrier and bit synchronization in data communications - A tutorial review," *IEEE Transactions on Communications,* vol. COM-28, no. 8, pp. 1107-21, 1980.

[35]   L.C. Palmer, S.A. Rhodes, S.H. Lebowitz, "Synchronization for QPSK transmission via communication satellites," *IEEE Trans. Comm.,* vol. COM-28, no. 10, pp. 1302-1314, 1980.

[36]   J.W. Modestino and S.Y. Mui, "Convolutional code performance in the Rician fading channel," *IEEE Trans. Comm.,* vol COM-24, no. 6, pp. 592-606, 1976.

[37]   F. Gagnon and D. Haccoun, "Bounds on the error performance of coding for non-independent Rician-fading channels," *IEEE Trans. Comm.,* vol. 40, no. 2, pp. 351-360, 1992.